

Recent developments in X-ray Talbot interferometry at ESRF-ID19

Timm Weitkamp^{ab*}, Irene Zanette^a, Christian David^c, José Baruchel^a, Martin Bech^d, Pascal Bernard^a, Hans Deyhle^e, Tilman Donath^c, Johannes Kenntner^f, Sabrina Lang^e, Jürgen Mohr^f, Bert Müller^e, Franz Pfeiffer^d, Elena Reznikova^f, Simon Rutishauser^c, Georg Schulz^e, Arne Tapfer^d and Jean-Paul Valade^a

^aEuropean Synchrotron Radiation Facility, Grenoble, France

^bSynchrotron Soleil, Gif-sur-Yvette, France

^cLaboratory for Micro- and Nanotechnology, Paul Scherrer Institut, Villigen, Switzerland

^dPhysik-Department (E17), Technische Universität München, Garching, Germany

^eBiomaterials Science Center, University of Basel, Basel, Switzerland

^fInstitute for Microstructure Technology, Karlsruhe Institute of Technology, Karlsruhe, Germany

ABSTRACT

In this paper we describe the design of different X-ray Talbot interferometers that have been built at the tomography beamline ID19 of the European Synchrotron Radiation Facility (ESRF) in Grenoble, France, and give a short review of performance characteristics, of current developments, and of the results obtained with these instruments so far. Among the applications so far, soft-tissue imaging has been a particular focus, as demonstrated in a recent paper by Schulz *et al.* (*J. Roy. Soc. Interface*, in press).

Keywords: X-ray tomography, X-ray phase contrast, coherence, Talbot interferometry, phase-stepping interferometry, synchrotron radiation, microtomography, phase retrieval

1. INTRODUCTION

X-ray Talbot interferometry (or, synonymously, X-ray grating interferometry) is a relatively young multimodal radiography method¹⁻⁴ yielding high-sensitivity differential phase-contrast images in two or three dimensions as well as scattering contrast (“dark-field” images).⁵

Originally developed at third-generation synchrotron sources, the method can be adapted to low-brilliance sources by suitable extensions.^{6,7} Beyond its applications in imaging and tomography, grating interferometry is applicable for in-situ wavefront monitoring^{3,8} and coherence characterization.^{9,10}

In an X-ray grating interferometer (Figure 1), a transmission grating structure G1 placed in the beam is used to induce a periodic modulation on the incident wavefront. The most efficient schemes in this context are those in which G1 only modulates the phase of the wavefront, but the amplitude modulation (i.e., the absorption in the grating lines) is negligible. The phase shift induced by the grating lines should be $\pi/2$ or π in the wavefront. The X-ray wavefront traveling downstream will retain the modulation; the positions of the planes with maximum intensity contrast of the modulation are determined by the Talbot self-imaging effect. For a grating with negligibly absorbing lines of period p_1 , the planes of maximum contrast for X rays of wavelength λ are given by

$$D_n = \frac{n}{2\lambda} \left(\frac{p_1}{\eta} \right)^2 \quad (n = 1, 3, 5, \dots), \quad (1)$$

where $\eta = 1$ for a $\pi/2$ -shifting grating, $\eta = 2$ for a π -shifting grating.¹¹ For an incident plane wave, the intensity modulation period will be p_1/η .

If the wavefront is distorted, so will be the modulation pattern. In this case, if the local distortions of the modulation can be detected, then the distribution of propagation angle of the wavefront across the plane can be determined (*deflectometry*

*E-mail: timm.weitkamp@synchrotron-soleil.fr

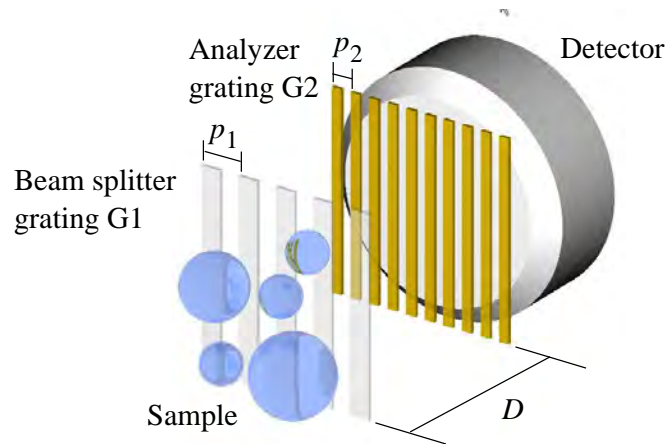


Figure 1: Setup of an X-ray grating interferometer used for radiography (schematic). The sample (here represented by spheres) is positioned upstream of the beam-splitter grating G1. A second grating G2, the analyzer, is placed at a distance D from G1. The image detector is positioned just downstream of G2. For details, including the choice of the periods p_1, p_2 of the gratings and on the inter-grating distance D , see text.

or *differential phase contrast*). If, in addition, the contrast variations of the modulation intensity can be detected, this will give a measure of the degree of transverse coherence of the beam (scattering contrast or dark-field imaging). Moreover, the averaged signal over an integral number of modulation periods can be used to retrieve the intensity distribution of the incident wavefront (i.e., a signal similar to the one that would be observed without the interferometer).

The sensitivity of a grating interferometer is intimately linked to the quantity D/p_1 , where D is the distance between G1 and the detection plane. For these reasons, building a sensitive grating interferometer usually requires the use of gratings with a period p_1 that is similar to or smaller than the pixel size (or size of the resolution element) of the detector used. This implies that the modulations from G1 cannot directly be resolved by the detector. A second grating G2, often called the *analyzer*, is then needed. The analyzer should have strongly absorbing structures with the same period as the (unperturbed) modulations in the detection plane. It will then act as a transmission mask, with the image detector placed closely downstream of G2. A two-grating interferometer of this kind can be used in moiré mode¹² or phase-stepping mode.^{4,13} While the former has the advantage of giving phase information in one shot, which is useful for wavefront sensing³ and fast imaging applications,¹⁴ the latter makes full use of the spatial resolution of the imaging system. In phase-stepping mode, one of the two gratings is scanned over one period in three or more steps. This procedure is called a *phase-stepping scan*. In moiré mode, the gratings are positioned with a small rotation angle relative to each other around the optical axis to obtain moiré fringes. A grating interferometer therefore usually needs a high-precision transverse motorized translation of one of the two gratings, and a rotation of one of the gratings around the beam axis.

When combined with X-ray tomography, the differential phase contrast capacity of X-ray Talbot interferometry yields quantitative reconstructions of the three-dimensional distribution $\delta(x, y, z)$ of the decrement of X-ray refractive index. The sensitivity of grating interferometric phase tomography has been proved to be as good as 2×10^{-10} (expressed in terms of the standard deviation of reconstructed values of δ in a homogeneous region of the sample).^{15–18}

2. TALBOT INTERFEROMETRY AT ID19

The insertion-device beamline ID19 is the only ESRF beamline fully dedicated to full-field parallel-beam imaging.^{19,20} Located on a low- β section of the storage ring, this long beamline delivers X rays over a wide energy range. The long distance between source and experimental station (150 m) results in a large beam size and high degree of transverse coherence. In its present configuration,^{20,21} ID19 has a maximum beam size of 40 mm (width) by 15 mm (height). X rays with photon energies ranging from 7 to over 100 keV are provided by a wiggler and three undulators. X rays can be used as a filtered white beam, monochromatized by a Si(111) double-crystal monochromator, or by a single-bounce multilayer. The broad range of experimental parameters and the good coherence properties of the beamline make it an instrument used for research in many fields, including materials science, biomedical applications²² and paleontology, in which the use of

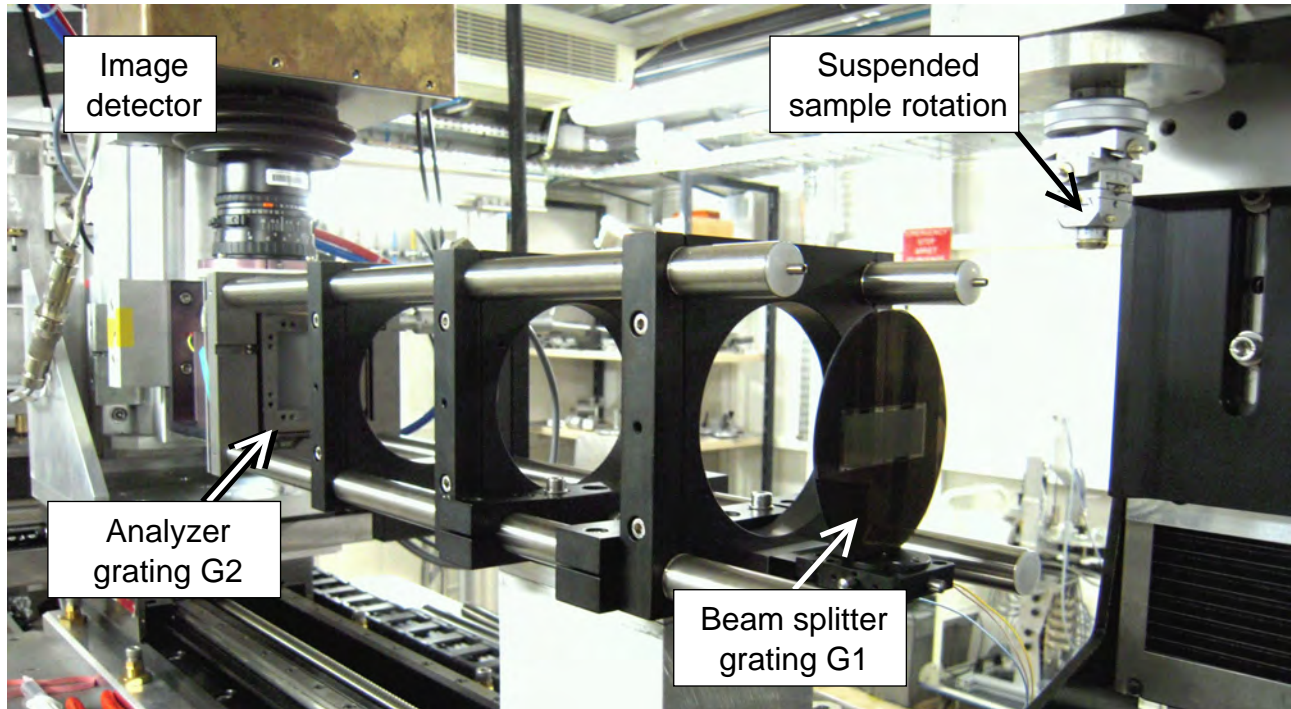


Figure 2: Photograph of the large-field interferometer setup on ID19.

X-ray phase contrast is particularly useful when material phases need to be discriminated that exhibit only subtle density differences.

ID19 has played an important part in the development of X-ray grating interferometry in Europe^{4,23} and continues to be one of the leading centers of activity in the field.^{15,17,24,25} A dedicated interferometer setup has been installed at the beamline starting in 2008.

3. TECHNICAL IMPLEMENTATION

Two modular interferometer hardware systems are available at ID19. Each of these two systems is used as a removable add-on on one of the two permanently-installed tomographs of the beamline.

Both interferometer systems are based on standard commercial optical mount systems that use four parallel rods to ensure orthogonality of the optical elements mounted on plates fixed to the rods. This concept, developed at the Paul Scherrer Institut, has proved flexible yet stable. The inter-grating distance in such an instrument can be varied manually. Different rod lengths are available to cover the full range of Talbot distances needed.

3.1. Large-field interferometer

The more commonly used of the two systems gives access to the full beam size at ID19. Based on the “Macrobench” series of optical mounts by the company Qioptiq Photonics GmbH & Co. KG (formerly Linos; Göttingen, Germany), it is optimized for high sensitivity (i.e., high density resolution) and large fields of view.

Mounted on the medium-resolution tomograph²⁰ of ID19, this interferometer system is typically used with the Si(111) double-crystal monochromator of the beamline. Figure 2 shows a picture of the device mounted.

The phase stepping scan axis is realized by a commercial piezo translation stage (HERA model series, by Physik Instrumente PI, Karlsruhe, Germany) with 100 μm travel range and 0.4 nm nominal resolution. The controller of the piezo stage is driven by an analog DC voltage in the range from 0 to 10 V, provided by the beamline electronics system. It is usually the beam-splitter grating G1 that is scanned.

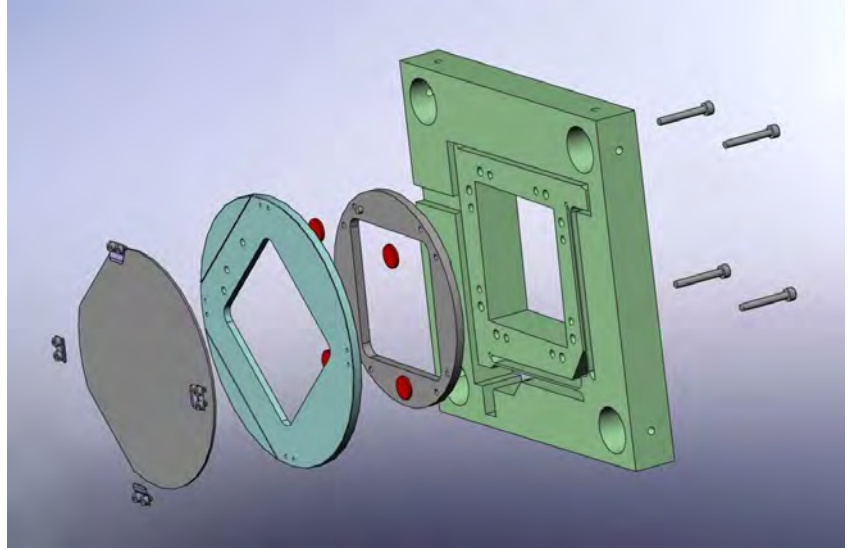
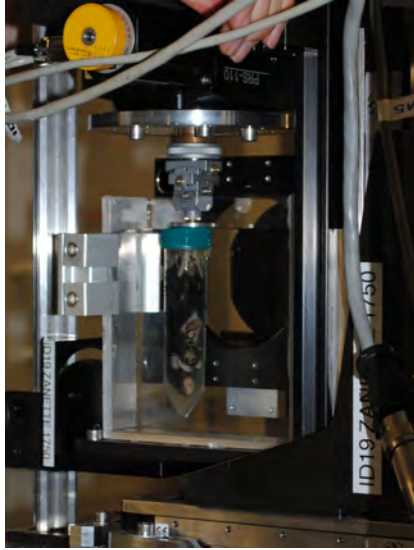


Figure 3: *Left:* Photograph of a sample (a mouse fixed in formalin, contained in a plastic tube container) mounted on the suspended rotation axis of the large-field interferometer, immersed in a water tank. *Right:* Flexure-hinge rotation stage and magnetic holder system for the analyzer grating.

The analyzer grating G2 can be rotated with a mechanism originally designed at the Paul Scherrer Institut. In this device, a system of flexure hinges acts as a reduction gear that allows rotation of the grating over a range of a few degrees. In the ESRF version, the rotation stage is made of aluminum and actuated by a conventional motorized screw (here, an MMS 19-25-HSM by Owis GmbH, Staufen, Germany). A magnetic holder, designed in-house, is used for easy mounting and pre-alignment of the analyzer grating (Figure 3, right panel).

To avoid artifacts in phase-stepping radiography and tomography, it is important that the periods p_1 and p_2 of the gratings G1 and G2 are adjusted to each other so that the fringe pattern created by G1 that impinges on G2 has a period of exactly p_2 . When this is the case, the gratings are said to be *divergence matched*.

For an incident wave that is perfectly plane, divergence matching is trivially obtained by choosing $p_2 = p_1/\eta$. However, in a real setup the finite distance L between the X-ray source and the interferometer makes it necessary to consider the radius of curvature of the X-ray wavefront, even at a long beamline such as ID19, where $L = 150$ m. The criterion for divergence matching is then

$$\frac{p_2}{p_1} = \eta \times \left(1 + \frac{D}{L}\right). \quad (2)$$

Since, in addition, a beam splitter grating is usable only at a single energy, in practice it is the period p_2 of the analyzer gratings that is kept fixed at a constant value for all experiments (in the case of ID19, $p_2 = 2.4 \mu\text{m}$). Each beam splitter grating either has a period p_1 tailored to fulfil Eq. 2, or it will be mounted with a slight tilt so that its projected period fulfils the condition. Beam splitter gratings are available for X-ray photon energies of 17.6, 23, and 35 keV. An experimental beam splitter with a design energy of 82 keV was also tested.

The large-field interferometer is generally used with a purpose-made tomography sample stage in which the sample is suspended so it can easily be immersed in a water tank during measurement. Immersion in a water tank with plane-parallel walls is used to avoid artifacts from the very strong phase gradient at the surface (or container wall, for samples in liquid environment) of the sample. At this surface, the DPC signal will exhibit phase jumps and other artifacts that are difficult to correct. Figure 3 (left) shows a picture of the setup with a sample mounted and inside the tank. Tanks of different geometries are available.

3.2. High-resolution, small-field interferometer

A second interferometer system for smaller fields, but higher spatial resolution, is currently used for in-house studies. It is based on the Microbench mounting system (Qioptiq). The grating rotation is provided by a rotation stage from the

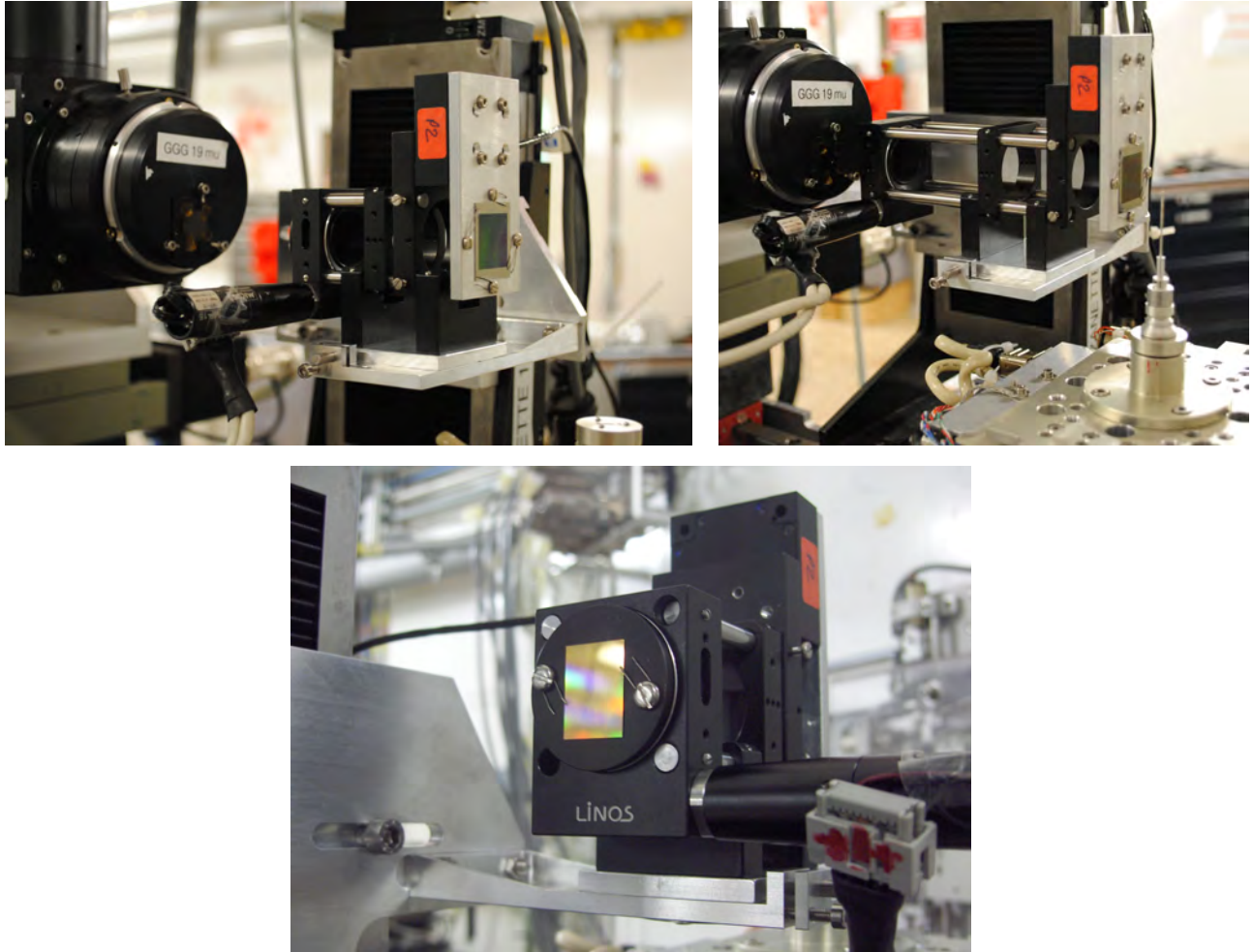


Figure 4: Photographs of HR interferometer setups on ID19. *Top row:* Note how different inter-grating distances D can be realized by choosing rods of different lengths. *Bottom:* View of the analyzer grating (here a grating made at the Paul Scherrer Institut).

Microbench system, actuated by a Micos MP-15 micropusher screw (Micos GmbH, Eschbach, Germany). This system, too, is based on a concept developed at the Paul Scherrer Institut and adapted to the ESRF environment. As in the large-field interferometer, a PI HERA piezo stage is used for phase stepping. Figure 4 shows interferometer setups realized with this system.

3.3. Data processing

The typical use case of the interferometers at ID19 is phase tomography in phase-stepping mode. The data processing chain is therefore tailored to this mode. The data processing chain essentially contains two steps:

1. The phase-stepping scans are analyzed using computer code written by the beamline staff, in IDL, the Interactive Data Language (ITT Visual Information Solutions, Boulder, Colorado, USA). The program performs an analytical or Fourier-based analysis (depending on the number of phase steps used in the scan) of the phase-stepping scans taken at each projection angle and extracts pseudo-absorption, differential phase contrast, and dark-field images for this projection angle. These processed projection images are then written to disk. If desired, the routine also outputs sinograms for each of the three contrast modalities.

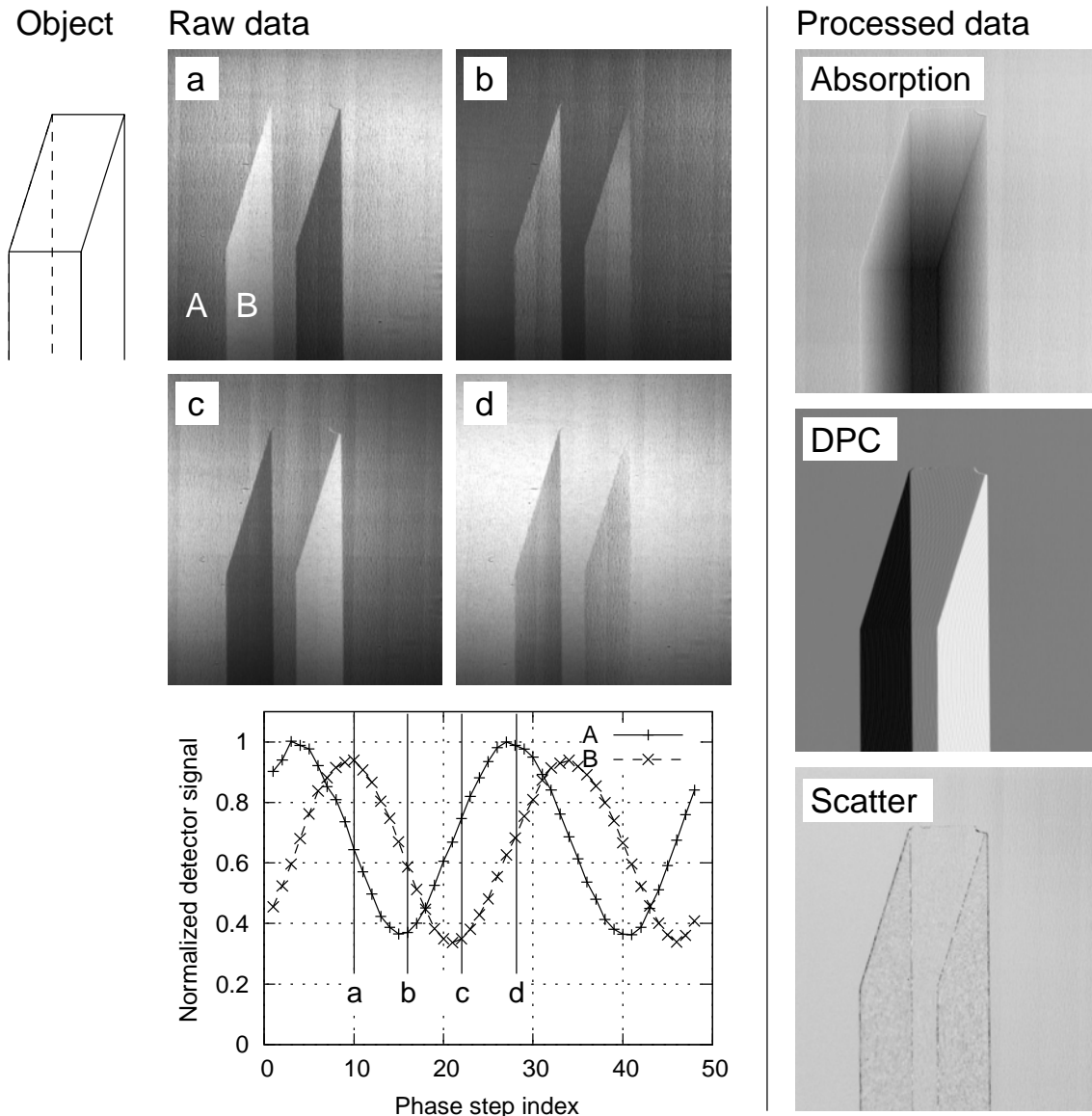


Figure 5: Phase-stepping interferometry. *Upper right, panels a through d:* raw data as recorded by the detector. The sample here was a square cylinder with a wedge-shaped tip, made of polymethyl methacrylate (acrylic glass). The raw images shown are four frames out of a total of 48 phase steps taken for this demonstration. The plot on the bottom shows the detector signal in two pixels A and B, as a function of the scan coordinate. The approximate positions of these pixels are indicated in panel a. The processed results (*right*) are the (pseudo-)absorption image, the differential phase contrast (DPC) image, and the “dark-field” (scatter) image, after application of flat-field and dark correction.

2. The tomographic reconstruction is then performed with the standard ESRF tomography reconstruction program PyHST, using the processed projection images generated in the pre-processing step. A Hilbert filter for processing of DPC data²⁶ is implemented in PyHST.

Figure 5 illustrates typical input and output images of step 1, the analysis of the phase-stepping scans. Figure 6, left, shows a phase tomogram obtained with the full analysis.

Another application example^{17,27} is shown in the right panel of the same figure. This study of the human cerebellum demonstrated how different strata in the brain can be discriminated in grating interferometric phase tomography. It also

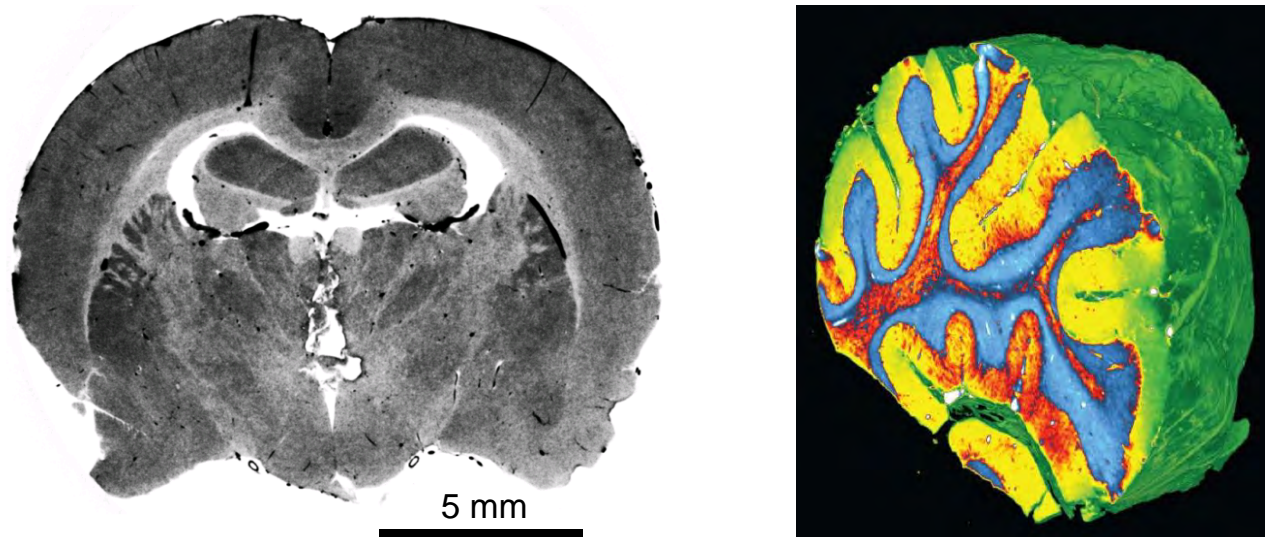


Figure 6: *Left:* Phase tomogram of a rat brain in buffered phosphate solution,²⁸ obtained with the large-field interferometer. *Right:* Three-dimensional false-color rendering of a human cerebellum, from a phase tomography dataset obtained with the interferometer. The full study is reported elsewhere.¹⁷

revealed structures presumed to be Purkinje cells. These cells have so far not been made visible with X rays without the use of staining agents.

4. TWO-DIMENSIONAL INTERFEROMETER

To complement the phase-contrast information obtained with a grating interferometer, it is possible to extend the concept by using two-dimensional structures as gratings G1 and G2, rather than the line gratings commonly used. A numerical study²⁹ shows that a suitable combination of two-dimensional grating structures can be obtained by superimposing two sets of, respectively, a π -shifting phase grating and an absorption grating, as shown in Figure 7 (left). We recently realized such

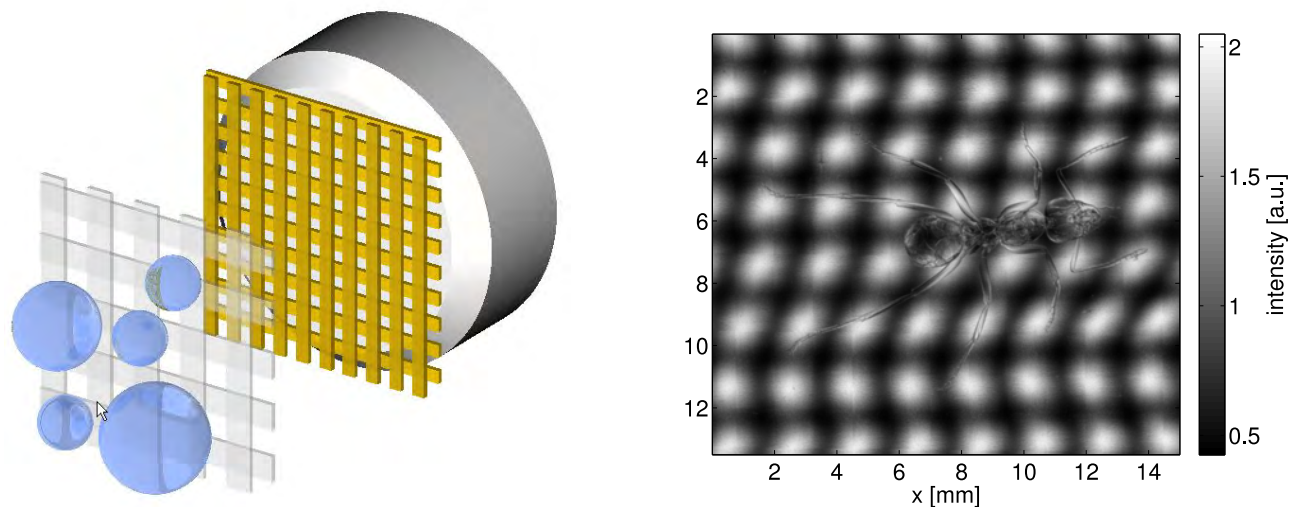


Figure 7: *Left:* Two-dimensional grating interferometer (schematic). *Right:* Raw projection radiograph of an ant in moiré mode obtained with a 2D interferometer on ID19.

a setup³⁰; the right panel in Figure 7 shows an image obtained in moiré mode with this device. Images in phase-stepping mode can also be obtained and yield phase projection images of far superior quality than those obtained with a one-dimensional interferometer.³⁰ A two-dimensional interferometer may prove particularly useful in cases where projection radiography is carried out (rather than tomography), for fast imaging and tomography in moiré mode,¹⁴ and for wavefront sensing applications at synchrotron facilities or other highly brilliant sources, such as X-ray free-electron lasers (XFELs).

5. CONCLUSIONS AND OUTLOOK

In a collaborative effort between several European laboratories, a modular X-ray Talbot interferometer setup was developed and installed at the beamline ID19 of the European Synchrotron Radiation Facility in Grenoble, France. The modular nature gives access to a wide range of energies and Talbot distances. Different sets of gratings are available. As a result of these developments, ID19 now provides a highly sensitive and reliable instrument for grating-based X-ray phase tomography, with an angular sensitivity of the DPC signal down to 10 nrad and a density resolution in phase tomography of down to $\Delta\delta \approx 2 \times 10^{-10}$.

The high spatial coherence, relatively large beam, and wide energy range of ID19 offer unique possibilities for the exploitation of this technique in the life sciences, paleontology, and materials science.

Among the ongoing developments are the access to higher X-ray energies and the development of two-dimensional interferometry. Access to high energies is crucial for the further development of synchrotron-based applications in paleontology, i.e., the imaging of fossilized organisms, and in view of the potential future use of interferometry in clinical imaging, such as head or body CT. Although these applications are not intended to be performed at synchrotron facilities, ID19 is an important test bed for the development and characterization of vital instrument components. The use of 2D gratings, rather than the current line gratings, and the development of related measurement and analysis strategies, can substantially improve data quality and phase reconstructions, particularly in cases where high accuracy of the results is a priority.

6. ACKNOWLEDGMENTS

The authors gratefully acknowledge Torben Rohbeck, Christian Grünzweig, Jens Bruder, Ana Diaz (PSI) and Martin Börner (KIT) for their contributions in past and present to the development of grating fabrication processes. Alessandro Mirone (ESRF) is acknowledged for the grating-specific additions to the PyHST tomography reconstruction software. José María Clement and Alejandro Homs (ESRF) have given excellent assistance in implementing the interferometer into the beamline controls system.

This work was carried out with the support of the Karlsruhe Nano Micro Facility (KNMF), a Helmholtz Research Infrastructure at Karlsruhe Institute of Technology (KIT). The European Synchrotron Radiation Facility (ESRF) has granted proposal beamtime (experiments MD-404, MD-407, MD-408, MI-983, MI-1058) for this project.

REFERENCES

1. C. David, B. Nöhammer, H. H. Solak, and E. Ziegler, "Differential x-ray phase contrast imaging using a shearing interferometer," *Appl. Phys. Lett.* **81**, pp. 3287–3289, 2002.
2. A. Momose, "Demonstration of X-ray Talbot interferometry," *Jpn. J. Appl. Phys.* **42**, pp. L866–L868, 2003.
3. T. Weitkamp, B. Nöhammer, A. Diaz, C. David, and E. Ziegler, "X-ray wavefront analysis and optics characterization with a grating interferometer," *Appl. Phys. Lett.* **86**, p. 054101, 2005. and Erratum.³¹
4. T. Weitkamp, A. Diaz, C. David, F. Pfeiffer, M. Stampanoni, P. Cloetens, and E. Ziegler, "X-ray phase imaging with a grating interferometer," *Opt. Express* **13**, pp. 6296–6304, 2005.
5. F. Pfeiffer, M. Bech, O. Bunk, P. Kraft, E. F. Eikenberry, C. Brönnimann, C. Grünzweig, and C. David, "Hard-X-ray dark-field imaging using a grating interferometer," *Nat. Mater.* **7**, pp. 134–137, 2008.
6. F. Pfeiffer, T. Weitkamp, O. Bunk, and C. David, "Phase retrieval and differential phase-contrast imaging with low-brilliance X-ray sources," *Nature Physics* **2**, pp. 258–261, 2006.
7. C. Kottler, F. Pfeiffer, O. Bunk, C. Grünzweig, J. Bruder, R. Kaufmann, L. Tlustos, H. Walt, I. Briod, T. Weitkamp, and C. David, "Phase contrast X-ray imaging of large samples using an incoherent laboratory source," *Physica stat. sol. A* **204**, pp. 2728–2733, 2007.

8. E. Ziegler, L. Peverini, I. V. Kozhevnikov, T. Weitkamp, and C. David, "On-line mirror surfacing monitored by X-ray shearing interferometry and X-ray scattering," *AIP Conf. Proc.* **879**, pp. 778–781, 2007.
9. F. Pfeiffer, O. Bunk, C. Schulze-Briese, A. Diaz, T. Weitkamp, C. David, J. F. van der Veen, I. Vartanyants, and I. K. Robinson, "Shearing interferometer for quantifying the coherence of hard X-ray beams," *Phys. Rev. Lett.* **94**, p. 164801, 2005.
10. A. Diaz, C. Mocuta, J. Stangl, M. Keplinger, T. Weitkamp, F. Pfeiffer, C. David, T. H. Metzger, and G. Bauer, "Coherence and wavefront characterization of Si-111 monochromators using double-grating interferometry," *J. Synchrotron Radiat.* **17**, pp. 299–307, 2010.
11. T. Weitkamp, C. David, C. Kottler, O. Bunk, and F. Pfeiffer, "Tomography with grating interferometers at low-brilliance sources," *Proc. SPIE* **6318**, pp. 63180S.1–10, 2006.
12. T. Weitkamp, A. Diaz, B. Nöhammer, F. Pfeiffer, M. Stampanoni, E. Ziegler, and C. David, "Moiré interferometry formulas for hard X-ray wavefront sensing," *Proc. SPIE* **5533**, pp. 140–144, 2004.
13. T. Weitkamp, A. Diaz, B. Nöhammer, F. Pfeiffer, T. Rohbeck, P. Cloetens, M. Stampanoni, and C. David, "Hard X-ray phase imaging and tomography with a grating interferometer," *Proc. SPIE* **5535**, pp. 137–142, 2004.
14. A. Momose, W. Yashiro, H. Maikusa, and Y. Takeda, "High-speed X-ray phase imaging and X-ray phase tomography with Talbot interferometer and white synchrotron radiation," *Opt. Express* **17**, pp. 12540–12545, 2009.
15. F. Pfeiffer, O. Bunk, C. Kottler, C. Grünzweig, C. David, M. Bech, G. Le Duc, A. Bravin, and P. Cloetens, "High-resolution brain tumor visualization using three-dimensional x-ray phase contrast tomography," *Phys. Med. Biol.* **52**, pp. 6923–6930, 2007.
16. J. Herzen, T. Donath, F. Pfeiffer, O. Bunk, C. Padeste, F. Beckmann, A. Schreyer, and C. David, "Quantitative phase-contrast tomography of a liquid phantom using a conventional x-ray tube source," *Opt. Express* **17**, pp. 10010–10018, 2009.
17. G. Schulz, T. Weitkamp, I. Zanette, F. Pfeiffer, F. Beckmann, C. David, S. Rutishauser, E. Reznikova, and B. Müller, "High-resolution X-ray tomography of a human cerebellum: Comparison of absorption and grating based phase contrast," *J. Roy. Soc. Interface* . in press.
18. I. Zanette, S. Lang, M. Langer, and T. Weitkamp, "Quantitative phase and absorption tomography with an X-ray grating interferometer and synchrotron radiation," in *Proceedings of XRM 2010, the 10th International Conference on X-Ray Microscopy*, *AIP Conf. Proc.* submitted.
19. P. Cloetens, W. Ludwig, J. Baruchel, J.-P. Guigay, P. Pernot-Rejmankova, M. Salome-Pateyron, M. Schlenker, J.-Y. Buffiere, E. Maire, and G. Peix, "Hard x-ray phase imaging using simple propagation of a coherent synchrotron radiation beam," *J. Phys. D* **32**, pp. A145–A151, 1999.
20. T. Weitkamp, P. Tafforeau, E. Boller, P. Cloetens, J.-P. Valade, P. Bernard, F. Peyrin, W. Ludwig, L. Helfen, and J. Baruchel, "Status and evolution of the ESRF beamline ID19," *AIP Conf. Proc.* **1221**, pp. 33–38, 2010.
21. T. Weitkamp, P. Tafforeau, E. Boller, P. Cloetens, J.-P. Valade, P. Bernard, F. Peyrin, W. Ludwig, L. Helfen, and J. Baruchel, "Parallel-beam imaging at the ESRF beamline ID19: current status and plans for the future," in *Proceedings of the 10th International Conference on Synchrotron Radiation Instrumentation (SRI '09)*, *AIP Conf. Proc.* , American Institute of Physics. in the press.
22. J. Baruchel, P. Bleuet, S. Bohic, A. Bravin, P. Coan, C. David, H. Elléaume, F. Estève, F. Peyrin, F. Pfeiffer, P. Suortti, O. Bunk, and T. Weitkamp, "State of the art and perspectives of biomedical imaging at the ESRF," *Synchrotron Rad. News* **21**(4), pp. 30–41, 2008.
23. C. David, T. Weitkamp, F. Pfeiffer, A. Diaz, J. Bruder, T. Rohbeck, A. Groso, O. Bunk, M. Stampanoni, and P. Cloetens, "Hard x-ray phase imaging and tomography using a grating interferometer," *Spectrochimica Acta B* **62**, pp. 626–630, 2007.
24. T. Weitkamp, O. Bunk, F. Pfeiffer, C. David, J. Bruder, and P. Cloetens, "X-ray phase radiography and tomography of soft tissue using grating interferometry," *Eur. J. Radiol.* **68**, pp. S13–S17, 2008.
25. B. Müller, S. Lang, M. Dominietto, M. Rudin, G. Schulz, H. Deyhle, M. Germann, F. Pfeiffer, C. David, and T. Weitkamp, "High-resolution tomographic imaging of microvessels," *Proc. SPIE* **7078**, pp. 70780B.1–10, Sept. 2008.
26. F. Pfeiffer, C. Kottler, O. Bunk, and C. David, "Hard X-ray phase tomography with low-brilliance sources," *Phys. Rev. Lett.* **98**, p. 108105, 2007.

27. G. Schulz, T. Weitkamp, I. Zanette, F. Beckmann, J. Herzen, F. Pfeiffer, S. Rutishauser, C. David, M. Müller-Gerbl, M. S. Imholz, and B. Müller, "Evaluating the microstructure of human brain tissues using synchrotron radiation," in *Developments in X-ray Tomography VII*, S. R. Stock, ed., *Proc. SPIE* **7804**, SPIE, (Bellingham, WA), 2010. submitted.
28. F. Pfeiffer, C. David, O. Bunk, C. Poitry-Yamate, R. Grütter, B. Müller, and T. Weitkamp, "High-sensitivity phase-contrast tomography of rat brain in phosphate buffered saline," *J. Phys. Conf. Series* **186**, p. 012046, 2009.
29. I. Zanette, C. David, S. Rutishauser, and T. Weitkamp, "2D grating simulation for X-ray phase-contrast and dark-field imaging with a Talbot interferometer," *AIP Conf. Proc.* **1221**, pp. 73–79, 2010.
30. I. Zanette, T. Weitkamp, T. Donath, S. Rutishauser, and C. David, "Two-dimensional X-ray grating interferometer." submitted.
31. T. Weitkamp, B. Nöhammer, A. Diaz, C. David, and E. Ziegler, "Erratum: X-ray wavefront and optics characterization with a grating interferometer," *Appl. Phys. Lett.* **86**, p. 119902, 2005.